Dynamics of Laser-Produced Plasmas through Time-Resolved Observations of the $2\omega_0$ and $\frac{3}{2}\omega_0$ Harmonic Light Emissions

Steven Jackel, Bruce Perry, and Moshe Lubin
Laboratory for Laser Energetics, College of Engineering and Applied Sciences, University of Rochester, Rochester, New York 14627
(Received 12 April 1976)

Time-resolved trajectories of the critical and quarter-critical densities were obtained through observation of plasma emissions at second and three-halves harmonics of the laser frequency. Characteristic behavior of the critical-density region is noted. Intensity histories of the plasma emissions were measured and compared to the incident pulse. The measurements were made during laser-fusion experiments where glass microballoon targets were irradiated with the 0.2-TW peak power output of a four-beam Nd:glass laser.

Knowledge of the plasma-density-profile history is important for an understanding of the laser-plasma interaction in laser-fusion experiments. The region of most intense laser-radiation–plasma interaction lies near the critical surface where the incident laser frequency ω_0 equals the plasma frequency $\omega_p=[(4\pi e^2/m)n_e]^{1/2}$. It is in this region that inverse bremsstrahlung absorption is strongest,[1] that resonant absorption occurs,[2,3] and in which many instabilities may be generated.[4]

In a previous paper[5] it has been shown that the critical and quarter-critical densities could be observed through the plasma emissions at the second and three-halves harmonics of the incident laser frequency. The $2\omega_0$ light was emitted from the critical electron density where $n_e=10^{21}$ cm^{-3} and the $\frac{3}{2}\omega_0$ light was emitted from the quarter-critical electron density where $n_e=2.5\times10^{20}$ cm^{-3}. The results consisted of time-integrated photographs which showed the maximum excursions of the critical and quarter-critical surfaces. A distinct separation between the peak $2\omega_0$ and $\frac{3}{2}\omega_0$ excursions was seen from which a "scale length," equal to the separation between the peak excursions, was measured.

Here we report time-resolved results obtained by imaging the plasma emissions through an electro-optic streak camera. Time-resolved trajectories of the critical and quarter-critical surfaces were measured. From these a time-resolved scale length was computed by subtracting the radius of the critical surface from that of the quarter-critical surface, i.e., $l\equiv r_{1/4\,cr}-r_{cr}$. In addition, the intensity time histories of the $2\omega_0$ and $\frac{3}{2}\omega_0$ plasma emissions and of the ω_0 incident pulse were obtained.

In the experimental arrangement, Fig. 1, glass microballoon targets were irradiated with the output of a four-beam Nd:glass laser.[6] Peak focusable outputs of the laser were in the range of 0.1 to 0.2 TW. The four beams were focused onto the target through four $f/2$ 20-cm focal-length aspheric lenses arrayed in a plane. Focal spots were 75–85 μm in diameter. The $2\omega_0$ and $\frac{3}{2}\omega_0$ emissions were viewed from a direction perpendicular to the plane of irradiation.

The equipment (Fig. 2) used for observing the plasma emissions allowed for the simultaneous observation of the $2\omega_0$ and $\frac{3}{2}\omega_0$ emissions with time-resolved measurements having one-dimensional spatial resolution and with time-integrated measurements having spatial resolution in two dimensions. The streaked $2\omega_0$ and $\frac{3}{2}\omega_0$ images were multiplexed spatially by placing the two images side by side on the streak-camera slits. The incident pulse was temporally multiplexed through control of the optical path lengths. Spatial resolution of the time-resolved images was 15 μm. Temporal resolution was 15 psec. Imaging through the streak-camera slits restricted the observations to a 5-μm-wide strip of plasma

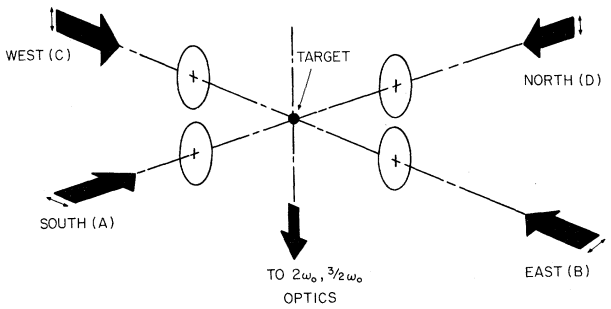

FIG. 1. The experimental arrangement. The four-beam Nd:glass laser output was focused onto the targets through four coplanar lenses. Plasma emissions were viewed from below.

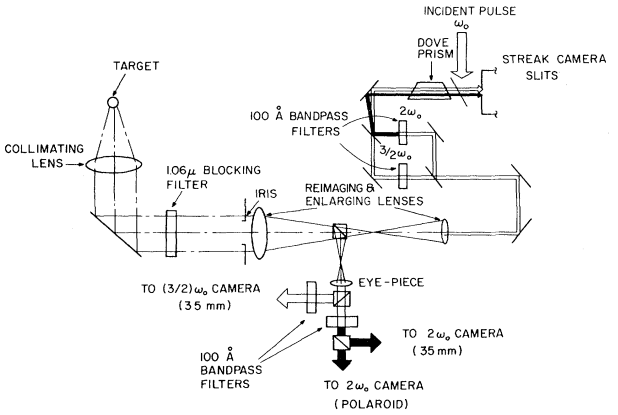

FIG. 2. Equipment for observing the plasma emissions.

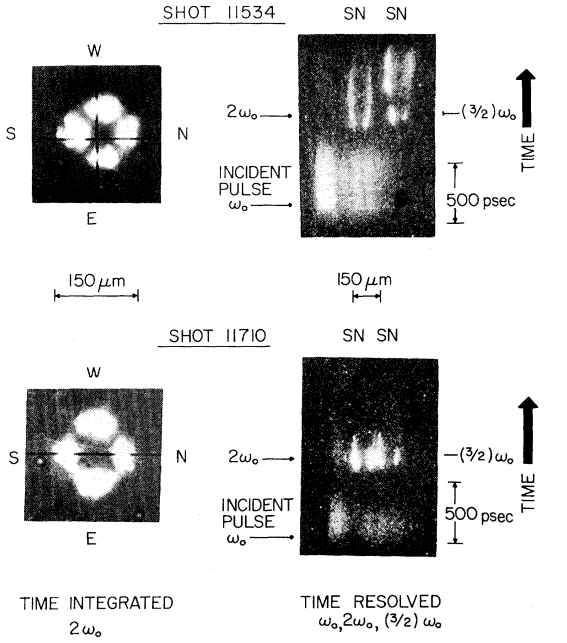

FIG. 3. Typical results. Time-integrated $2\omega_0$ image showing the symmetry of illumination. Streak photos show the incident pulse followed by the plasma emissions. Shot data: 11 534-target radius, 42 μm; energy on target, 50 J; peak laser power on target, 0.13 TW; and energy in ions, 3 J. 11 710-target radius, 49 μm; energy on target, 36 J; peak laser power on target 0.14 TW; and energy in ion, 3 J.

parallel to the south-north axis.

Figure 3 shows the results from two shots. The pictures on the left are the time-integrated $2\omega_0$ photographs. Four distinct sectors can be seen, each with a lateral extent about equal to the vacuum focal spot of the laser beam. To the right are the time-resolved streak photographs with the incident pulse followed by the $2\omega_0$ and $\frac{3}{2}\omega_0$ images. Each harmonic image consists of two streaks since only light passing through the camera slits is recorded. Each streak is produced by emissions from the region of interaction between the plasma and the south or north laser beam.

The trajectories of the critical and quarter-critical surfaces were obtained by taking microdensitometer traces along the spatial dimension of the $2\omega_0$ and $\frac{3}{2}\omega_0$ images at 5-psec intervals. The instantaneous positions of the emitting surfaces were located at the outer edges of the streaks. Each image has a finite thickness due to the fact that the image is a two-dimensional projection of a three-dimensional emitting surface. The emitting surface is the region of interaction between the critical or quarter-critical layer and the laser light. The thickness of the projection and the intensity distribution within it is a sensitive function of the laser-beam–plasma interaction. The outer edge of the intensity distribution does not have this sensitive dependence.

The critical and quarter-critical surface trajectories of the plasma facing the south beam for the two shots in Fig. 3 are shown in Fig. 4(a). The lines are least-squares curve fits to the data of a polynomial series up through fourth order. At the onset of the $2\omega_0$ emissions the initial critical-surface expansion velocities were 4×10^7 cm/sec for both shots. Initial expansion velocities on the order of 10^7 cm/sec were typical of most shots. Within 100 psec the critical surface reached a position which remained nearly constant for most of the duration of the incident laser pulse. The extent of critical surface expansion to this plateau region tended to be smaller for faster risetime pulses. While the critical surface remained stationary the quarter-critical surface continued to expand. It was during this time that a scale length developed [Fig. 4(b)]. In shot 11 534 (top row in Fig. 4) the peak expansion of the quarter-critical surface occurred after the critical surface had started moving inwards. In this case the scale length continually increased with time. In shot 11 710 (bottom row in Fig. 4) the peak expansion of the quarter-critical surface occurred while the critical surface was in its stationary phase. After this point the scale length decreased. Similar contractions of scale length have been observed in other shots. Note that in shot 11 710 the plasma emissions did not start at the beginning of the incident laser pulse. At the

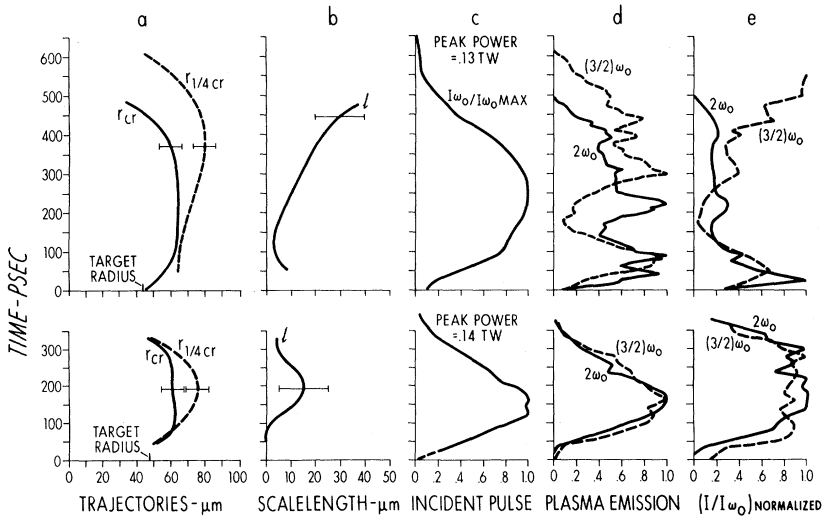

FIG. 4. Data taken from the streak photographs of Fig. 3. Time $t = 0$ psec is set at start of the incident pulse (top row, 11 534; bottom row, 11 710). (a) Critical and quarter-critical surface trajectories; (b) evolution of the scale length; (c) history of the incident pulse; (d) intensities of the plasma emissions; (e) emission intensities divided by the intensity of the incident pulse.

beginning of the plasma emissions the critical and quarter-critical surfaces were, however, near the initial target position. The behavior of these surfaces during the first 40 psec of the laser pulse is unclear.

"Flares" in the $2\omega_0$ and $\frac{3}{2}\omega_0$ emission were observed on several shots. These were short duration extensions of the light patterns beyond the relatively smooth outer edges of the emitting surfaces. These flares lasted for less than 50 psec and had lengths of up to 50 μm. Flares did not occur simultaneously in the plasma facing both beams. Flares occurring simultaneously at both frequencies were not observed.

In addition to obtaining the critical and quarter-critical trajectories the streaked $2\omega_0$ and $\frac{3}{2}\omega_0$ results provided time histories of the emission intensities. These were obtained by taking microdensitometer traces parallel to the time axis on the streak photo with a slit height that just covered the plasma emission from one of the beams. Density on film was converted to intensity through shot-to-shot film calibration. The streak camera was measured to be linear over a dynamic range of 15. Figure 4(c) gives the incident-pulse time history and 4(d) gives the time histories of the plasma emissions. The plots are plots of intensity normalized to the peak intensity. Time $t = 0$ psec has been set at the start of the laser pulse.

In shot 11 710 the intensity of the plasma emissions in the south beam tended to follow the intensity of the incident pulse. This was not the case in 11 534 where, as seen in Fig. 4(d), a dip occurred in the $2\omega_0$ and $\frac{3}{2}\omega_0$ intensities. Dips in the $2\omega_0$ and $\frac{3}{2}\omega_0$ intensities uncorrelated to drops in the incident pulse intensity were common. They generally occurred in the plasma produced by both of the opposing beams. Whether the dips were due to frequency shifts outside of the ~100 Å windows of the interference filters or due to actual intensity drops is as yet unknown. During a single shot, the emission histories for the plasma facing the two beams were not necessarily the same. Thus in Fig. 3, for shot 11 710, the north-beam intensity profile had a full width at half-maximum duration 0.6 of that for the south beam.

To investigate the mechanisms for $2\omega_0$ and $\frac{3}{2}\omega_0$ production perpendicular to the laser axis, simple power-law relationships were sought. In Fig. 4(e) the functions $(I_{2\omega_0}/I_{\omega_0})$ and $(I_{3\omega_0/2}/I_{\omega_0})$ have been plotted in an attempt to understand the relevant parameters. Comparison of $(I_{3\omega_0/2}/I_{\omega_0})$ and the scale-length plots in 3(b) shows that the function $(I_{3\omega_0/2}/I_{\omega_0})$ is largest when the scale lengths are long. In 11 534, after the first 150 psec, both the scale length and $(I_{3\omega_0/2}/I_{\omega_0})$ increase with time. In 11 710 the two quantities are near their peak values at 200 psec.

The $2\omega_0$ intensities do not appear to have a scale length dependence. If in 11 710, where the $(I_{2\omega_0}/I_{\omega_0})$ correlation is good, a power-law dependence of the form $I_{2\omega_0} = \text{const} I_{\omega_0}{}^N$ is assumed

then it is found that $N \simeq 1.2$ for the south beam and 2.4 for the north beam. In 11 534 the correlation is not as good but a value of $N \simeq 1.2$ is obtained.

In conclusion it can be said that the time and spatially resolved $2\omega_0$ and $\frac{3}{2}\omega_0$ measurements have begun to provide the data necessary for an understanding of the laser-beam–plasma interactions occurring in the region of the critical surface. The spatial resolution of the $2\omega_0$ and $\frac{3}{2}\omega_0$ streaked results provides critical and quarter-critical surface trajectories. This gives information on the hydrodynamics of the ablation region. Time-resolved scale lengths provide information for absorption studies. Intensity histories of the plasma emissions should yield information on the processes that lead to the plasma emissions.

This work is supported by the Laser Fusion Feasibility Project at the University of Rochester.

[1]R. Kidder, in *Physics of High Energy Density*, edited by P. Caldirola and H. Knoepfel (Academic, New York, 1971).

[2]K. Estabrook, E. Valeo, and W. Kruer, Phys. Fluids 18, 1151 (1975).

[3]D. Forslund, J. Kindel, K. Lee, E. Lindman, and R. Morse, Phys. Rev. A 11, 679 (1975).

[4]D. DuBois, in *Laser Interaction and Related Plasma Phenomena*, edited by H. Schwarz and H. Hora (Plenum, New York, 1974), Vol. 3, pt. A.

[5]S. Jackel, J. Albritton, and E. Goldman, Phys. Rev. Lett. 35, 514 (1975).

[6]M. Lubin, E. Goldman, J. Soures, L. Goldman, W. Friedman, S. Letzring, J. Albritton, P. Koch, and B. Yaakobi, in *Proceedings of the Fifth International Conference on Plasma Physics and Controlled Nuclear Fusion Research, Tokyo, Japan, 1974* (International Atomic Energy Agency, Vienna, Austria, 1975), Vol. II, pp. 459–477.

Synchrotron Radiation from the ATC Tokamak Plasma*

D. A. Boyd, F. J. Stauffer, and A. W. Trivelpiece
Department of Physics and Astronomy, University of Maryland, College Park, Maryland 20742
(Received 8 March 1976)

The synchrotron radiation emitted from the adiabatic toroidal compressor (ATC) tokamak plasma along a major radius was measured over a band of frequencies (35 GHz $< f <$ 450 GHz with resolution $f/\Delta f \approx 2$ and rise time $\tau < 10$ μsec) that included the electron cyclotron frequency and its first few harmonics. The radiation is at least 50% polarized ($\vec{E}_{\text{wave}} \perp \vec{B}$). Radiation due to runaway electrons increases sharply and coincidentally with the appearance of positive spikes in the loop voltage and decays exponentially after the onset of an $m = 2$ oscillation in the plasma.

Costley and co-workers[1,2] recently reported on measurements of the spectral distribution and the polarization of the synchrotron radiation emitted by the CLEO and TRF tokamak plasmas (parallel and perpendicular to the major radius) over a frequency band (30 GHz $< f <$ 450 GHz) that included the electron cyclotron frequency ($\omega_c = eB/m$) and its first few harmonics. They found, contrary to expectation based on theoretical analysis of simple plasma models,[3-5] that (1) the intensity was greater than would be expected for plasmas with the electron temperatures produced by these devices, (2) the intensity was spatially isotropic, and (3) the radiation was unpolarized. Their apparatus consisted of a scanning Michelson interferometer and Putley[6] detector combined to make a Fourier-transform spectrometer. This system, which has the advantage of excellent frequency resolution ($\Delta f \approx 20$ GHz, i.e., $f/\Delta f = 10$ at 200 GHz), required 10 msec to scan the frequency range of interest and produce a Fourier transform of the spectral distribution of the observed radiation. This meant that they were able to obtain valid spectra only for those stable tokamak discharges for which the plasma parameters were nearly constant over a 10-msec interval.

This Letter reports measurements of the synchrotron radiation emitted by the adiabatic toroidal compressor[1] (ATC) tokamak plasma over the same band of frequencies, with an apparatus that had a worse frequency resolution ($f/\Delta f \sim 1-2$), but much better time resolution (< 10 μsec) than that used by Costley and co-workers.[1,2] Consequently, we concentrated on effects occurring on a time scale shorter than 10 msec and obtained a number of results not discussed in the present theory of synchrotron radiation in tokamas. We hope they will act as a stimulus to new theoreti-

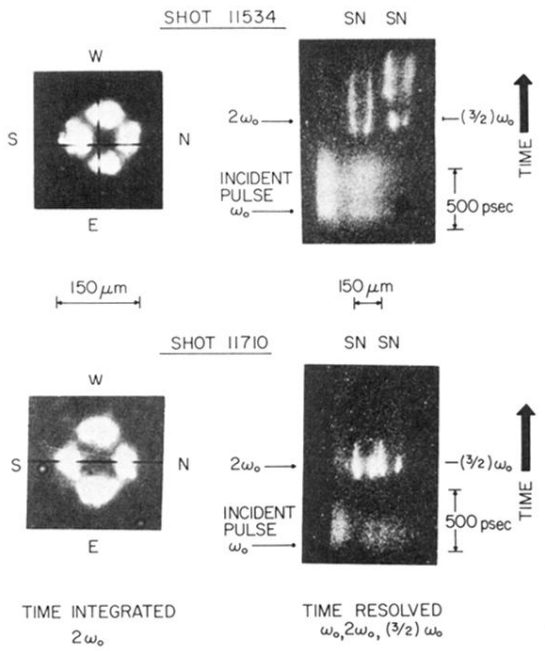

FIG. 3. Typical results. Time-integrated $2\omega_0$ image showing the symmetry of illumination. Streak photos show the incident pulse followed by the plasma emissions. Shot data: 11 534-target radius, 42 μm; energy on target, 50 J; peak laser power on target, 0.13 TW; and energy in ions, 3 J. 11 710-target radius, 49 μm; energy on target, 36 J; peak laser power on target 0.14 TW; and energy in ion, 3 J.